Depolarized and Fully Active Cathode Based on Li(Ni$_{0.5}$Co$_{0.2}$Mn$_{0.3}$)O$_2$ Embedded in Carbon Nanotube Network for Advanced Batteries

Zhongzhen Wu,[†] Xiaogang Han,[‡] Jiaxin Zheng,[†] Yi Wei,[†] Ruimin Qiao,[§] Fei Shen,[‡] Jiaqi Dai,[‡] Liangbing Hu,[‡] Kang Xu,[∥] Yuan Lin,[†] Wanli Yang,[§] and Feng Pan*,[†]

[†]School of Advanced Materials, Peking University Shenzhen Graduate School, Shenzhen 518055, China

[‡]Department of Materials Science and Engineering, University of Maryland, College Park, Maryland 20742, United States

[§]Advanced Light Source, Lawrence Berkeley National Laboratory, Berkeley, California 94720, United States

[∥]U.S. Army Research Laboratory, Adelphi, Maryland 20783, United States

S Supporting Information

ABSTRACT: Improving battery capacity and power is a daunting challenge, and in Li-ion batteries positive electrodes often set the limitation on both properties. Layered transition-metal oxides have served as the mainstream cathode materials for high-energy batteries due to their large theoretical capacity (∼280 mAh/g). Here we report a significant enhancement of cathode capacity utilization through a novel concept of material design. By embedding Li(Ni$_{0.5}$Co$_{0.2}$Mn$_{0.3}$)O$_2$ in the single wall carbon nanotube (CNT) network, we created a composite in which all components are electrochemically active. Long-term charge/discharge stability was obtained between 3.0 and 4.8 V, and both Li(Ni$_{0.5}$Co$_{0.2}$Mn$_{0.3}$)O$_2$ and CNT contribute to the overall reversible capacity by 250 and 50 mAh/g, respectively. The observed improvement causes significant depolarization within the electrodes through the CNT network system. Additionally, the depolarization provides the ideal template to understand the solid reaction mechanism of Li(Ni$_{0.5}$Co$_{0.2}$Mn$_{0.3}$)O$_2$ by demonstrating well-defined two-stage delithiation kinetics consistent with first-principle calculations, which would be otherwise impossible. These results deliver new insights on both practical designs and fundamental understandings of battery cathodes.

KEYWORDS: Depolarization, full-active cathode, low functionalized CNT, NCM523, capacity, delithiation kinetic
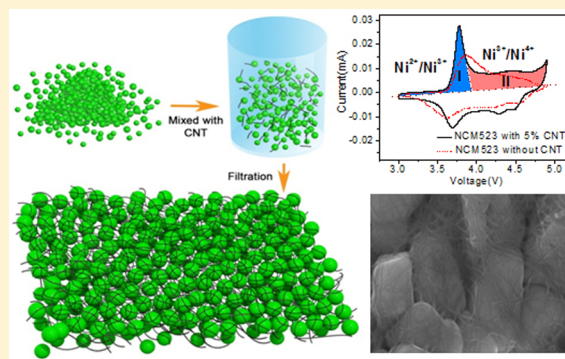
Demands for lithium (Li)-ion batteries currently range from portable electronics to large-scale applications such as stationary energy storage systems and automotive power sources.[1,2] Layered Li transition metal oxides have served as the mainstream cathode materials for high-energy batteries due to their large theoretical capacity (∼280 mAh/g) compared with their olivine- or spinel-structured counterparts.[3] In particular, two variations of ternary layered LiNi$_x$Co$_y$Mn$_z$O$_2$ (0 ≤ x, y, z < 1) (called as NCM), that is, LiNi$_{1/3}$Co$_{1/3}$Mn$_{1/3}$O$_2$ and LiNi$_{0.5}$Co$_{0.2}$Mn$_{0.3}$O$_2$ have been successfully adopted in commercial Li-ion batteries on the expectation of their promising electrochemical properties.[4] Nevertheless, numerous works have verified that a highly discounted reversible capacity of about 200 mAh/g could be utilized.[5−7]

One reason for this underutilization is the poor accessibility of the potential active species in the narrow electrochemical potential range of 4.2−4.5 V, which has been deliberately set in order to avoid the structural transformation that is anticipated to happen at a higher cutoff limit of 5.0 V and the consequent rapid capacity fading thus induced.[8,9] However, in fact, this transformation into spinel or rock salt phase was only observed in a thin surface layer of the NCM particle at these high

voltages, while the Li-rich phase remained intact in the core[10,11] and the consequential nonuniform distribution of electrochemical potential on the NCM particles. Carbon nanotubes (CNTs) have been usually mixed with active anode or cathode materials to resolve the issues of sluggish electron transport kinetics and rate performances.[12] Among those efforts, the free-standing, binder-free three-dimensional (3D)-carbon nanotube networks prepared by filtration or deposition are considered the ideal higher electronic conducting structure to make the electrodes depolarization for such purposes.[13−15] Carbon nanotube networks have already been used previously with layered cathode materials for the purpose of improving the electronic conductivity with focus placed on rate performance in these efforts.[16,17] However, efforts via CNT network paid less attention to the release of the latent capacity of NCM materials that cannot be accessed otherwise in the conventional cathode structure. Interestingly, functionalized CNT was reported to demonstrate extra capacity in the potential range

of cathode materials,[18,19] hinting at a new concept of all-active cathode constructed with only functional CNT and NCM materials.

Here, we report a composite cathode material NCM523/CNT for advanced Li ion batteries, wherein all components are electrochemically active and effectively depolarized. NCM523 was intimately embedded into the low-functionalized single wall CNTs to form a stand-alone electrode with much improved performance, which does not contain any inert components that conventional composite cathode materials do, such as polymer binder or carbon conductive additives. In this design, the CNT network simultaneously served as an electron transport pathway as well as an active cathode ingredient besides NCM523, showing reversible electrochemical activity during the Li ion battery operation in the presence of a high voltage electrolyte. We found that the polarization of NCM523 particles was significantly reduced due to the conductive network structure, resulting in about a 25% increase in the reversible capacity and an obvious improvement in the cycling and rate performance compared with that prepared through conventional approaches. Additionally, well-defined two-stage delithiation process in the NCM523/CNT composite electrodes could be clearly observed as a result of the facilitated mass and electron transport processes. Employing first principle method, we took advantage of this ideal template to understand the solid chemical reaction mechanism in NCM523 and calculated the diffusion barriers of Li$^+$ in different local environments around Ni—O, Co—O, and Mn—O in comparison with the experimental data, where the kinetics of the two-stage delithiation process were deciphered according to the structure—properties relationship in the layer Li-ion battery. The clear fundamental mechanism gives us a useful guidance to the future design and applications of the layered NCM cathodes.

The NCM523 particles in this work were prepared by the coprecipitation method as described in the previous references,[20] which consisted of 5−10 μm spherical secondary particles constructed upon submicron-sized primary particles with a narrow size distribution in the range of 300−500 nm as shown in Supporting Information Figure S1. The free-standing, binder-free NCM523/CNT composite cathode was achieved by the vacuum filtration using a sodium dodecyl benzenesulfonate (SDBS) solvent, where the CNT and the NCM523 particles were dispersed with a ratio of 5:95 as illustrated in Figure 1. As a comparison, two types of NCM523 composites with carbon black (CB) and polymer binder (PVDF) with or without CNT were also prepared by the conventional slurry/coating method, hereafter denoted as slurry NCM523/CNT/CB and NCM523/CB, respectively.

For each of these cathode composites, their unique hierarchical structures and electric contact microenvironment would be expected to provide a unique electronic conductivity and mass transfer kinetics, which are in turn responsible for the respective electrochemical performances. Figure 2 showed the SEM micrographs of these cathode composites. The secondary particle of NCM523, agglomerated with 300−500 nm primary particles as building blocks, are revealed to be intimately embedded in the 3D CNT network and homogeneously distributed. As schematically illustrated in Figure 1, the 3D netting tightly interweaves around each NCM523 particle and forms a well-connected microenvironment as shown in Figure 2a,b and its inset. In sharp comparison, according to Figure 2c,d the microenvironments of NCM523 particles as prepared from
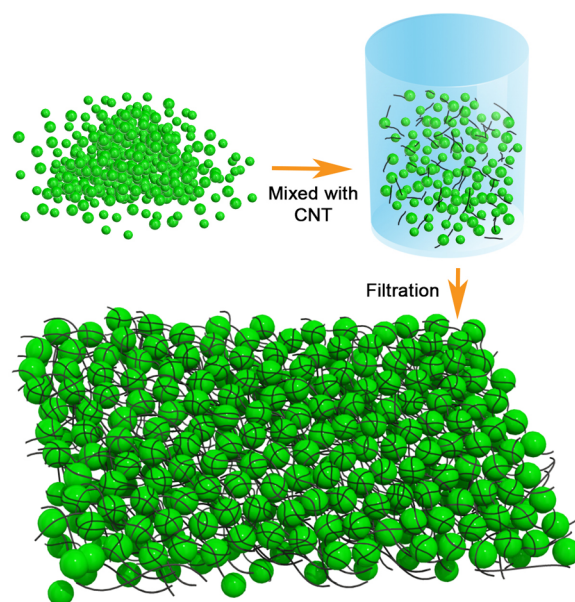

Figure 1. The schematic of the preparation process for the NCM/CNT free-standing film cathodes. The cathodes are obtained from vacuum-filtration of the mixture of NCM particles and CNT in aqueous solution. The 1D nanomaterial of CNT wraps on the NCM particle surfaces and is interwoven through the gaps between NCM particles, forming an electric network with NCM particles embedded.

slurries with CNT/CB or CB were shown to possess random electric contacts as well as crevices of 300 nm gaping. Nevertheless, between the two slurry samples the presence of CNTs in NCM523/CNT/CB sample still established certain effective wiring around the NCM particles as shown in Figure 2c, which might ensure a better electric conductive environment than that in the slurry NCM523/CB composite without CNT. In contrast with these two slurry samples, where tortuosity for electron transfer would certainly ensue as the result of the inhomogeneous electric connection to induce polarization for the electrodes, significant decrease in electrical resistance by about 2 orders of magnitude was found in the binder-free 3D-networked NCM523/CNT composite, as shown in Figure 3a. Thus, the CNT in NCM523/CNT electrodes helps solve the interparticle polarization between the secondary particles (Figure 2b) and the intraparticle polarization of the single secondary particle, which is constructed with 300−500 nm primary particles to be "wired" with the CNT-network (Figure 2a). This improved electric conductivity along with the well-wired particles should lead to significant depolarization in the electrode when electron and mass migrate under the electric field, and a facile electrochemical reaction kinetic is thus expected in the 3D solid phase.

The electrochemical performances of the prepared cathode composites in a high voltage electrolyte are displayed in Figure 3b,c and Supporting Information Figures S2 and S3. The fluorinated high-voltage electrolyte, formulated with mono-fluoroethylene carbonate (FEC) and a highly fluorinated ether (HFE) along with 5 mM additive tris(hexafluoro-iso-propyl)-phosphate (HFiP) ensures that a stable interphase is formed on the highly oxidizing surface of the cathode when it is charged beyond 4.5 V.[21,22] The electrochemical depolarization in the binder-free NCM523/CNT composite is strongly suggested by the very narrow overpotentials shown in Supporting Information Figure S4. Note that an extra contribution to the
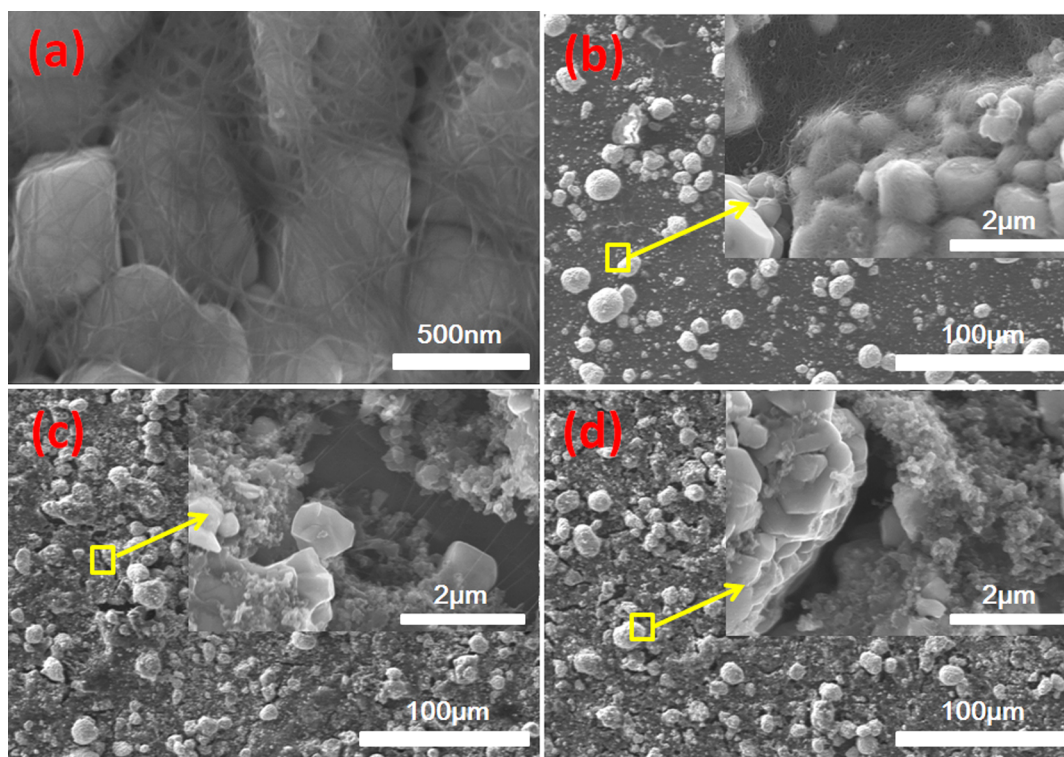
Figure 2. SEM images for the NCM cathodes prepared in various configurations. NCM cathodes obtained by filtration with 5% CNT (a,b) and also by slurry method with (c) and without 5% CNT added (d). The inserts in panels b−d are the magnified images of the corresponded areas marked in the yellow squares.

capacity by the CNT has been subtracted from the binder-free NCM523/CNT and the slurry NCM523/CNT/CB composites, which are calculated according to and described in Supporting Information Figure S5. Supported by the high-voltage electrolyte, all these samples showed the higher charge current in the first cycle in the wider charging voltage range of 3.0−4.8 V, as shown in Figure 4a−d and Supporting Information Figure S5c, which was attributed to the oxidation of CNT and the formation of the solid electrolyte interphases (SEI) as shown in Supporting Information Figure S6. The corresponding processes were not detected in the following cycles, and after the initial several cycles a consistent capacity contribution from the CNT eventually stabilized at about ∼50 mAh/g, as shown in Supporting Information Figure S5. This could originate from two different sources, that is, the electrochemical double-layer capacitance contribution between 3.0 and 4.8 V, calculated to be about 10.8 mAh/g (based on the CV of CNT in Supporting Information Figure S5c), and the Faradaic processes at higher charge/discharge voltage.[18,19] For the oxidation case, there is the oxidation peak from 4.2 to 4.8 V to suggest the formation of Li_2CO_3 from functional groups −COOH of the CNT;[23] for reduction case, there is a broad peak around 3.8−4.6 V (Supporting Information Figure S5d). The possibility of another Faradaic mechanism, that is, the intercalation of anions into graphitic carbon,[24,25] should be excluded here, because single wall CNTs should not provide intercalation interstitials as graphitic structures do, although the similar potential where the anion-intercalation occurred (4.8−5.0 V) was employed in these experiments, as shown in Figures 3b,c, and 4. Thus, the CNTs in the binder-free NCM523/CNT served dual purposes, that is, depolarizing the active NCM523 cathode material by creating a homogeneously 3D electrical

wiring environment and contributing an extra reversible capacity as part of the fully active cathode.

Much improved rate performance and capacity utilization, as exemplified by an average capacity of 250 mAh/g between 3.0 and 4.8 V when supported by the high voltage electrolyte (seen in Methods), was achieved in the 3D netting NCM523/CNT as shown in Figure 3. With the capacity contribution from CNT considered, the total capacity of the full-active cathode achieves 261.8 mAh/g. In comparison, the capacity of the slurry NCM523/CB composites remained at the level of ∼200 mAh/g in the same voltage ranges, which is comparable with previous reports (the Supporting Information Table S1). It should be emphasized here that the capacity of the slurry NCM523/CNT/CB composite was 225 mAh/g, higher than that of the slurry NCM523/CB composite by ∼10%, apparently due to the presence of CNT. To further validate the reproducibility of the superior electrochemical performances from 3D-networked NCM523/CNT composite, more than 10 parallel samples were prepared independently, which demonstrated capacities from 235 to 262 mAh/g (Supporting Information Figure S3), a healthy range due to the mass variation of the inhomogeneous dispersion of NCM523 particles during filtration of the cathode film. Thus, the higher reversible capacity in the binder-free NCM523/CNT composite is confirmed with high confidence. The first 60 cycles of the binder-free NCM523/CNT composite and the two slurry composites were compared at charge/discharge rates between 0.1C to 4C as shown in Figure 3c, which shows higher rate capabilities with 36% capacity decrease from 0.1C to 1C for the composites with CNT compared with 43.7% for the slurry sample without CNT. The same distinction in cycling stability as well as capacity utilization exists for these composites up to 160 cycles as shown in Supporting Information Figure S2a. Although the
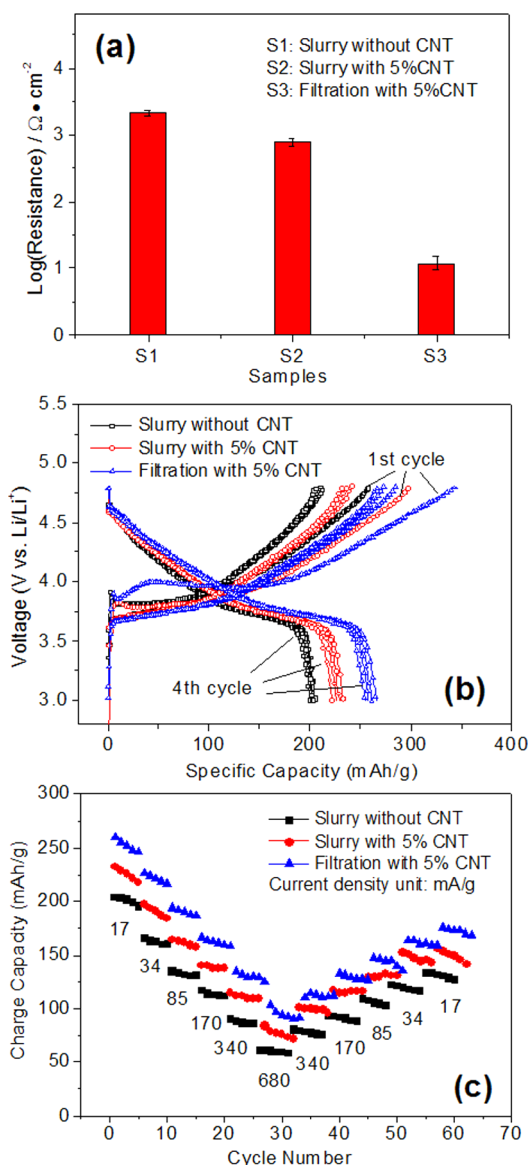
Figure 3. Resistance electrochemical performances of the three as-prepared $Li(Ni_{0.5}Co_{0.2}Mn_{0.3})O_2$ cathodes: (a) Resistance between the two sides for the as-prepared cathodes using different configurations. (b) The voltage profiles for the first four charge and discharge cycles between 3 and 4.8 V using Li as both counter and reference electrode. (c) Rate performance with charge/discharge current densities varied from 17 to 680 mA/g.

capacity still fades during these cycles, the amount of latent capacity released in binder-free NCM523/CNT composite indicated that the depolarization approach is effective; further improvement in cycling stability could be achieved through surface stabilization techniques such as prevention of transition metal dissolution by ALD (seen Supporting Information Figure S2b).

An additional benefit of this depolarization comes from the fundamental aspect. It was well-known that the charging process of NCM-like cathode materials should consist of two distinct stages of delithiation that correspond to the oxidation of Ni^{2+} to Ni^{3+} and then Ni^{4+}. In reality, those two processes were almost never clearly differentiated due to the sluggish kinetics of the electrochemical reactions. Specifically, the polarization within the cathode materials forces the reactions

to proceed with sufficient overpotentials so that significant overlapping exists between the two processes. However, the presence of CNT-network in the binder-free NCM523/CNT composite creates a microenvironment that is so well-wired electronically that a drastically different electrochemical behavior ensues. Figure 4 showed the cyclic voltammetry of these NCM composite cathodes, among which well-separated two-stage delithiation processes in binder-free NCM523/CNT electrode (Figure 4c) clearly stood out. This differentiation of the two-stage delithiation process was never observed previously and provides a unique template to understand the dynamics as well as mass and electron transport mechanism in NCM cathode materials.

For a better comparison, the CV curves of the NCM523/CNT and the slurry NCM523/CB in the fourth cycle were overlain as shown in Figure 4d. In sharp contrast to the well-separated delithiation processes of NCM523/CNT, characterized with the sharp peak of exponentially increased current (blue) and the flat plateau (pink), the slurry composites exhibited a broad peak followed by a wide shoulder, indicative of sluggish kinetics of both processes and significant over-lapping. Apparently, the reduced electrical resistance and resultant depolarization effectively equilibrated the potential within the binder-free NCM523/CNT composite with the nominal potential applied, so that delithiation could start at a lower potential with sharper feature as shown in Figure 4d. The charge/discharge rate benefitted from the same depolarization effect as shown in Figure 3.

The kinetics of the two-stage delithiation process in the NCM523 cathode was investigated by the first principle calculation (seen in Methods) and crystal structure analysis. The different diffusion barriers of Li^+ around $Ni-O$, $Co-O$, and $Mn-O$ in the NCM523 matrix were calculated by the first principle method as shown in Figure 5a. The diffusion barrier of the Li^+ around $Ni-O$ was found to be much lower than those of Li^+ around $Co-O$ or $Mn-O$. The calculation result suggests that in the NCM523 the Li^+ ions near $Ni-O$ sites can delithiate first due to its lower energy barrier, which matches the first delithiation step with the lowest threshold of potential as shown in Figure 4d (stage-I, blue). In contrast, those Li^+ ions in the vicinity of Co and Mn need more driving force to diffuse due to the higher energy barriers, which corresponds to the second delithiation step with the higher threshold potential as shown in Figure 4d (stage-II, pink).

Previous studies have verified that the main contributions to the reversible NCM capacity is from complete Ni redox reaction, while the Co and Mn remains electrochemically inert according to in situ X-ray absorption spectroscopic (XAS) and X-ray absorption fine structure (EXAFS) investigations.[26,27] Because of the similar electronic energy levels of Ni^{3+} and Ni^{4+}, the redox reactions of Ni^{2+}/Ni^{3+} and Ni^{3+}/Ni^{4+} usually cannot be distinguished clearly and the dynamic is missed.[28,29] Here we adopt a simplified model in which the transition metal atoms are arranged with certain ordering in the compounds.[30] We have calculated the total energies of three different transition metal ordering models and found that the most energetically favorable structure is the one shown in Supporting Information Figure S7. The cell voltage is calculated according to the following equation[31]

$$V = -\left\{ \frac{E(Li_{x+\Delta x}R) - E(Li_x R)}{dx} - E(Li) \right\}$$
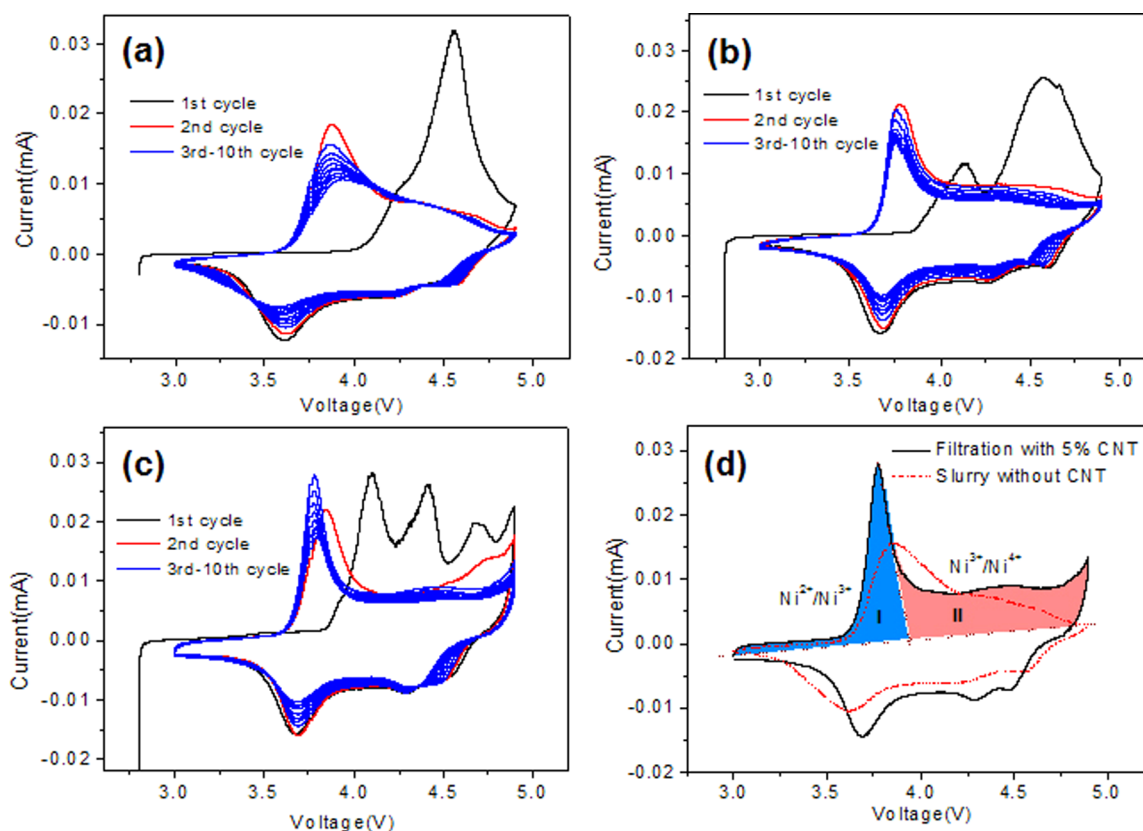
(1)

Figure 4. Cyclic voltammograms (CV) of the as-prepared NCM cathodes. (a) Slurry NCM without CNT, (b) slurry NCM with 5% CNT, and (c) filtration NCM with 5% CNT. For the electrochemistry tests, lithium metal disks are used as both counter and reference electrodes. All the scan rates are 0.05 mV/s. (d) CV curve comparison for the slurry NCM (dash line) and filtration NCM (solid line) cathodes. For convenience, the two delithiation stages in the filtration NCM cathode are colored in blue (I, Ni^{2+}/Ni^{3+}) and pink (II, Ni^{3+}/Ni^{4+}).

Where $E(Li_xR)$ and $E(Li_{x+dx}R)$ stand for the total energy before and after dx lithium ions is removed from LiR compound per formula unit, and $E(Li)$ is the total energy of lithium metal. Figure 5b shows the capacity versus cell voltage profile of $Li_{(1-x)}Ni_{0.5}Co_{0.2}Mn_{0.3}O_2$ cathode materials after shifting up 0.8 eV, and it agrees well with the experimental results (the fourth cycle of the filtration sample at the current density of 17 mA/g). When the voltage increases to 4.8 V, the capacity reaches 250 mAh/g, which is comparable with the average capacities obtained as shown in Supporting Information Figure S3, further confirming the depolarization of the 3D-netting NCM523/CTN because the model in simulation does not consider any polarization factor. Note that the delithiation capacity of the measured NCM523/CNT sample as shown in Figure 5b is still lower than the simulated value between 3.6 and 3.9 V (the stage-I) and less capacity was extracted at the higher charging potential (the stage-II as shown in Figure 4d). Nevertheless, the simulation results reasonably support the depolarization effect and the two-stage delithiation mechanism of the NCM materials.

We also calculate the magnetic moments of nickel ions with the lithium concentration $x = 0$ and $x = 0.5$. Ni^{2+}, Ni^{3+}, and Ni^{4+} are expected to have a total electron spin count of ± 2, ± 1, and 0 (in units of 1/2 μB), respectively.[32] Around $x = 0$, our calculated magnetic values for nickel atoms are around 1.5, indicating that the nickel ions possess a Ni^{2+} oxidation state. During the delithiation process, when x reaches to $x = 0.5$, the magnetic values for most of the nickel ions are around 0.7, which shows that the oxidation state for most of the nickel ions

are changed from Ni^{2+} to Ni^{3+}. Interestingly, the magnetic values for the left little part of the nickel ions are around 0.1, indicating that the Ni^{4+} has appeared. It should be noted that the moment around nickel is slightly below what is expected for Ni^{2+} and Ni^{3+}. This can be attributed to the orbital overlap between the 3d states of nickel and oxygen 2p states.[33]

The two different delithiation stages are also discussed according to the delithiation capacity, the crystal structure, and the change of the charging potential by analyzing both experimental and theoretical results in Figure 5. During the first stage, about half of the total Li^+ ions in NCM523 (140 mAh/g in capacity) was delithiated in a narrow range of 0.2 V around 3.7 V according the experimental data, and in the narrow range of less than 0.1 V around the 3.7 V according the calculation data because the model in simulation does not have polarization factor (Figure 5b), which can be attributed to the delithiation of Ni sites based on the crystal structure as shown in Figure 5c, where about half of total Li^+ ions in NCM523 are located near Ni within a short distance (d_{Li-Ni}) of about 2.79 Å (the detailed distances are displayed in the Supporting Information Figure S8). The first delithiation stage with charging potential (3.7 ± 0.1 V) closely matches the process of delithiation stage-I found in the CV curve shown in Figure 4d (pink color), in which most of nickel ions are changed from Ni^{2+} to Ni^{3+} according to the above calculation. In contrast, at the second stage the remaining half of total Li^+ ions in the NCM523 was delithiated only under the much larger driving force as evidenced by the higher charging potential of 3.9−5.0 V (Figure 5b), which may be attributed to delithiation of Co-
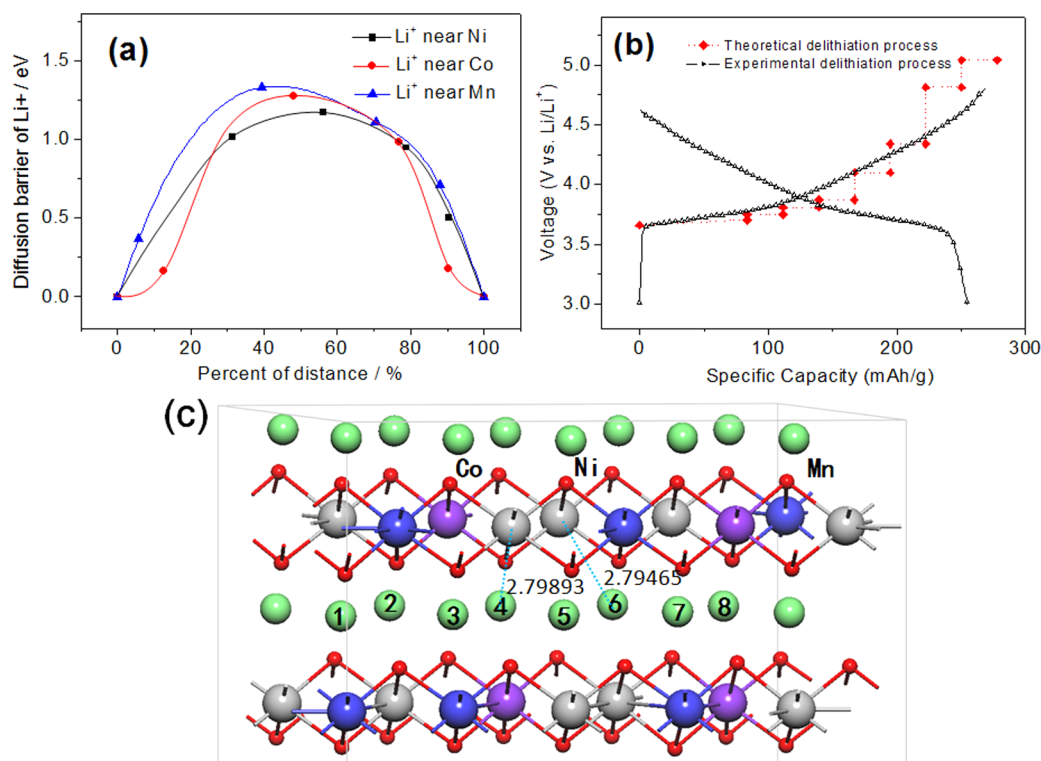
Figure 5. Analysis of the two-stage delithiation kinetics and illustration of NCM crystal structure. (a) Diffusion energy barriers of Li+ around Ni−O, Co−O, and Mn−O in NCM523. (b) Voltage curves of NCM cathode calculated based on the first-principle method, and the experimental data obtained from the filtration NCM/CNT cathodes are shown in it for comparison. (c) Layered crystal structure of the NCM particles with the distance between Li+ and transition metal atoms. The lithium atoms are numbered and the transition metal atoms are colored for identification.

and Mn-sites (Figure 5c) due to their higher diffusion energy barriers as shown in Figure 5a. Interestingly, it should be noted from Figure 4d that the current is almost constant to the charging potential from 3.9 to 4.8 V.

In conclusion, we have developed a fully active and depolarized composite cathode material based on NCM523 particles embedded in the interwoven 3D CNT network, which serves the dual functions of both storing Li ions as the active materials and providing the superhighway for the electron and Li ion migration. Because of the effective depolarization introduced by the CNT network, release of the latent capacity in the NCM523 materials that cannot be accessed otherwise and the relative improvements in the cycling and rate performance at high cutoff voltage of 4.8 V were achieved. Additionally, the well-defined two-stage delithiation kinetics in NCM materials was enabled by the depolarization and observed clearly. According to the first principle calculation of the NCM layer crystal structure, the dynamic transportation of the Li+ in the two-stage delithiation process is revealed, which is the consequence of the difference in Li diffusion barriers created by their association with the local transition metal sites. The design philosophy for the composite cathode structured with the active additive CNT lend us further inspiration to the optimized all-active cathode materials with depolarization for the next generation energy storage batteries and vehicle batteries.

■ ASSOCIATED CONTENT

Ⓢ Supporting Information

Details of the method section, the morphology, XRD patterns, resistance, electrochemical performances of the prepared samples and the pure CNT samples, the TEMs and soft X-ray data of the interface layer, and layered crystal structure simulated by the first principle method. This material is available free of charge via the Internet at http://pubs.acs.org.

■ AUTHOR INFORMATION

Corresponding Author

*E-mail: panfeng@pkusz.edu.cn. Tel/Fax: +86-755-26033200.

Author Contributions

This work was initiated by Z.W., F.P., and L.H. The experiment and electrochemical data was performed by Z.W., X.H., and F.S. The soft X-ray spectra was collected by R.Q. and W.Y. The electrolyte was provided by K.X. The calculation was performed by J.Z. and Y.W. The data analysis was performed by Z.W., F.P., Y.L., W.Y., and J.Z. The manuscript was written by Z.W., F.P., W.Y., J.Z., K.X., and J.D.

Z.W. and X.H. contributed equally.

Notes

The authors declare no competing financial interest.

■ REFERENCES

(1) Tarascon, J.-M.; Armand, M. *Nature* **2001**, *414*, 359−367.

(2) Armand, M.; Tarascon, J. M. *Nature* **2008**, *451*, 652−657.

(3) Ohzuku, T.; Makimura, Y. *Chem. Lett.* **2001**, *30*, 642−643.

(4) Wang, L.; Li, J.; He, X.; Pu, W.; Wan, C.; Jiang, C. *J. Solid State Electrochem.* **2009**, *13*, 1157−1164.

(5) Sun, Y.-K.; Myung, S.-T.; Kim, M.-H.; Prakash, J.; Amine, K. *J. Am. Chem. Soc.* **2005**, *127*, 13411−13418.

(6) Sun, Y.-K.; Myung, S.-T.; Park, B.-C.; Prakash, J.; Belharouak, I.; Amine, K. *Nat. Mater.* **2009**, *8*, 320−324.

(7) Xiao, J.; Chernova, N. A.; Whittingham, M. S. *Chem. Mater.* **2009**, *22*, 1180−1185.

(8) MacNeil, D. D.; Lu, Z.; Dahn, J. R. *J. Electrochem. Soc.* **2002**, *149*, A1332−A1336.

(9) Kim, J.-M.; Chung, H.-T. *Electrochim. Acta* **2004**, *49*, 937−944.

(10) Jung, S.-K.; Gwon, H.; Hong, J.; Park, K.-Y.; Seo, D.-H.; Kim, H.; Hyun, J.; Yang, W.; Kang, K. *Adv. Energy Mater.* **2014**, *4*, 1300787.

(11) Wu, L.; Nam, K.-W.; Wang, X.; Zhou, Y.; Zheng, J.-C.; Yang, X.-Q.; Zhu, Y. *Chem. Mater.* **2011**, *23*, 3953−3960.

(12) Landi, B. J.; Ganter, M. J.; Cress, C. D.; DiLeo, R. A.; Raffaelle, R. P. *Energy Environ. Sci.* **2009**, *2*, 638−654.

(13) Luo, S.; Wang, K.; Wang, J.; Jiang, K.; Li, Q.; Fan, S. *Adv. Mater.* **2012**, *24*, 2294−2298.

(14) Perera, S. D.; Patel, B.; Nijem, N.; Roodenko, K.; Seitz, O.; Ferraris, J. P.; Chabal, Y. J.; Balkas, K. J., Jr *Adv. Energy Mater.* **2011**, *1*, 936−945.

(15) Chew, S. Y.; Ng, S. H.; Wang, J.; Novak, P.; Krumeich, F.; Chou, S. L.; Chend, J.; Liu, H. K. *Carbon* **2009**, *47*, 2976−2983.

(16) Li, X.; Kang, F.; Shen, W. *Electrochem. Solid-State Lett.* **2006**, *9*, A126−A129.

(17) Ban, C.; ali, Z.; Wu, Z.; Kirkham, M. J.; Chen, L.; Jung, Y. S.; Payzant, E. A.; Yan, Y.; Whittingham, M. S.; Dillon, A. C. *Adv. Energy Mater.* **2011**, *1*, 58−62.

(18) Itkis, M. E.; Perea, D. E.; Niyogi, S.; Rickard, S. M.; Hamon, M. A.; Hu, H.; Zhao, B.; Haddon, R. C. *Nano Lett.* **2003**, *3*, 309−314.

(19) Lee, S. W.; Yabuuchi, N.; Gallant, B. M.; Chen, S.; Kim, B.-S.; Hammond, P. T.; Yang, S.-H. *Nat. Nanotechnol.* **2010**, *5*, 531−537.

(20) Lee, M.-H.; Kanga, Y.-J.; Myung, S.-T.; Sun, Y.-K. *Electrochim. Acta* **2004**, *50*, 939−948.

(21) Zhang, Z.; Hu, L.; Wu, H.; Weng, W.; Koh, M.; Redfern, P. C.; Curtiss, L. A.; Amine, K. *Energy Environ. Sci.* **2013**, *6*, 1806−1810.

(22) Cresce, A. v. W.; Xu, K. *J. Electrochem. Soc.* **2011**, *158*, A337−A342.

(23) Liu, Y.; Wang, R.; Lyu, Y.; Li, H.; Chen, L. *Energy Environ. Sci.* **2014**, *7*, 705−714.

(24) Seel, J. A.; Dahn, J. R. *J. Electrochem. Soc.* **2000**, *147*, 892−898.

(25) Read, J. A.; Cresce, A. v. W.; Ervin, M. H.; Xu, K. *Energy Environ. Sci.* **2014**, *7*, 617−620.

(26) Tsai, Y. W.; Hwang, B. J.; Ceder, G.; Sheu, H. S.; Liu, D. G.; Lee, J. F. *Chem. Mater.* **2005**, *17*, 3191−3199.

(27) Liu, X.; Wang, D.; Liu, G.; Srinivasan, V.; Liu, Z.; Hussain, Z.; Yang, W. *Nat. Commun.* **2013**, *4*, 3568.

(28) Deb, A.; Bergmann, U.; Cramer, S. P.; Cairns, E. J. *J. Appl. Phys.* **2005**, *97*, 113523.

(29) Shaju, K. M.; Rao, G. V. S.; Chowdari, B. V. R. *Electrochim. Acta* **2002**, *48*, 145−151.

(30) Thackeray, M. M.; Kang, S.-H.; Johnson, C. S.; Vaughey, J. T.; Benedek, R.; Hackney, S. A. *J. Mater. Chem.* **2007**, *17*, 3112−3125.

(31) Ceder, G.; Ven, A. V.; Marianetti, C.; Morgan, D. *Modell. Simul. Mater. Sci. Eng.* **2000**, *8*, 311−321.

(32) Kresse, G.; Furthmüller, J. *Phys. Rev. B* **1996**, *54*, 11169−11186.

(33) Hwang, B. J.; Tsai, Y. W.; Carlier, D.; Ceder, G. *Chem. Mater.* **2003**, *15*, 3676−3682.